Preprint
UCRL-JC-139367

X-Ray Backlighting for the National Ignition Facility

O. L. Landen, D. R. Fraley, S. G. Glendinning, L. M. Logory, P. M. Bell, J. A. Koch, F. D. Lee, D. K. Bradley, D. H. Kalantar, C. A. Back, R. E. Turner

This article was submitted to
13th Topical Conference on High Temperature Plasma Diagnostics, Tucson, Arizona, June 19-23, 2000

July 25, 2000

U.S. Department of Energy

Lawrence
Livermore
National
Laboratory

X-Ray Backlighting for the National Ignition Facility*

O. L. Landen, D.R. Fraley, S.G. Glendinning, L.M. Logory, P.M. Bell, J.A. Koch, F.D. Lee, D.K. Bradley, D.H. Kalantar, C.A. Back, R.E. Turner

Lawrence Livermore National Laboratory
P.O. Box 5508, Livermore, CA 94551

Abstract

X-ray backlighting is a powerful tool for diagnosing a large variety of high-energy-density phenomena. Traditional area backlighting techniques used at Nova and Omega cannot be extended efficiently to NIF-scale. New, more efficient backlighting sources and techniques are required and have begun to show promising results. These include a backlit-pinhole point-projection technique, pinhole and slit arrays, distributed polychromatic sources, and picket-fence backlighters. In parallel, there have been developments in improving the data SNR and hence quality by switching from film to CCD-based recording media and by removing the fixed-pattern noise of MCP-based cameras.

*Work performed under the auspices of the U.S. Department of Energy by the University of California Lawrence Livermore National Laboratory under contract number W-7405-ENG-48.

I. Introduction

X-ray backlighting refers to the technique of radiographing transient phenomena in high-density materials. It is a powerful method of measuring hydrodynamic evolution of a material subject to external pressures, such as those created by x-ray[1-6] or laser ablation[7-9]. When the backlighter is either monochromatic or spectrally resolved by the imaging instrument, information on the opacity or equation-of-state of a material can also be gleaned[10-19].Transient, picosecond- to nanosecond-duration x-ray backlighter sources emanate from plasmas created by the interaction of high-intensity laser beams with foils[20-29]. Imaging is usually provided by one of three methods:

1. Pinholes[30-36] (for 2D imaging) or slits[4,35,37] (for 1D imaging) are placed between the backlit sample and detector.
2. A point source of x rays is created that casts a shadow of the sample at the detector[22,23,38-40].
3. X-ray optics such as curved mirrors[35,41-44] and Fresnel lenses[45] cast a backlit image at the detector.

The intrinsic spatial resolution depends on a combination of the detector resolution and the pinhole diameter, point-source size, or quality of the figure of the optic, respectively[30,35]. The effective resolution, however, as limited by data noise, can be worse. Noise arises from insufficient photons collected per resolution element (shot noise), or spatial nonuniformities in the instrument response.

In the first section of this article, "Imaging Techniques" we review the strengths and weaknesses of the first two backlighting geometries, especially in the context of extrapolating to NIF scale. Because the third backlighting method, utilizing x-ray optics, is inherently expensive and calibration-intensive, it has not been able to accommodate the wide variety of high-energy-density and inertial confinement fusion (ICF) experiments demanding timely, quantitative backlighting at arbitrary photon energy. Hence, we will not further discuss this

third option, but rather endeavor to show how improvements in the first two techniques can make them at least as valuable for the National Ignition Facility (NIF) as they have been at Nova and Omega. For example, we propose variants on these backlighting geometries that should improve the backlighter efficiency for some current experiments by factors of up to 100. Recent results from Nova and Omega with the new techniques are also presented as proof of principle.

In the second section, "Backlighter Sources", we discuss how the backlighter source efficiency can be increased by using spatially distributed, broader-bandwidth sources. Supporting results from Nova are also presented. In the third section, "Detectors", we discuss the choice of detector, particularly with respect to the data signal-to-noise ratio (SNR). We present recent results showing significant improvements in data SNR by switching from film to CCD as the final recording medium and by correcting postshot for fixed pattern noise on framing camera data. We conclude by discussing the experiments we have planned at Omega for further validating these new backlighting concepts, which will be essential for NIF.

II. Imaging Techniques

We first review the two standard backlighting techniques commonly known as area backlighting and point-projection backlighting. We explain why current area backlighting is impractical at NIF scale, and why current point-projection backlighting has not and will not become a mainstay technique at any size facility. We then present a variant on the current point-projection technique, backlit pinhole backlighting, which combines the best features of both traditional techniques while providing a potentially more efficient x-ray source for all future experiments. Methods for further increasing the photon-collection efficiency by using redundant imaging apertures are also discussed.

a) Area Backlighting

For area backlighting, imaging is provided by a pinhole or slit placed between the backlit sample and the detector, as shown in Figure 1a. The backlighter source size by simple geometry must be at least as large as the sample transverse dimensions. There are three principal advantages to this technique:

1. The spatial resolution is determined by a fixed entity, a pinhole or slit that can be easily precharacterized and can almost always be shielded or distanced sufficiently from the target and backlighter environment to avoid closure.
2. Multiple images from slightly different lines of sight can be cast on a single detector using a single backlighter spot. If each image is gated at a separate time while the backlighter laser beam is on, then a sequence of images is obtained in time, typically 16 for a wide variety of experiments at Nova and Omega. Alternatively, those 16 images could be recorded on a static detector such as x-ray film or an x-ray CCD and then summed for improving SNR. In this case, the temporal resolution is set by the backlighter x-ray duration.
3. The cooling of the backlighter plasma due to energy loss out the edges of the laser spot is mitigated by having a large spot.

We now consider how area backlighting scales from Nova and Omega to NIF. Consider an experiment seeking to backlight a sample driven by a given radiation temperature hohlraum environment. NIF will have $\approx 4^2$x more power than Nova or Omega, hence NIF will be able to drive a 4x larger hohlraum to the same temperature. If the sample is also scaled up by 4x in size and 4^2x in area, than the area backlighter must also be scaled up by 4^2x in area. Assuming for the moment a fixed-photon-energy backlighter, keeping the backlighter x-ray intensity fixed is equivalent to keeping the backlighter laser intensity fixed. Therefore, under the current assumptions, the backlighter laser power must be 4^2x larger. Stated differently, the fraction of laser power apportioned to backlighting would be fixed as we transition from Nova to NIF. Because we typically use 10 to 20% of the beams at Nova for backlighting, we would require

10 to 20% of the beams on NIF. However, this is overly optimistic. First, because of the ≈ 4x longer drive durations possible with NIF for fixed hohlraum temperature, the samples are likely to be thicker, hence requiring higher photon energy backlighting, which requires higher backlighter intensities and power. Second, for a given desired spatial and temporal resolution and number of collected photons per resolution element, the required backlighter x-ray intensity is fixed only if the imaging detector is kept at the same stand-off distance as at Nova. This in general will not be possible when considering how diagnostic damage and debris concerns scale to NIF[46]. For example, for fixed debris and x-ray fluence, the stand-off distance would be $4^{1.5}$x further at NIF. For the same number of collected photons per resolution element, the required backlighter x-ray and hence laser intensity would be 4^3x greater. Therefore, the combination of higher backlighter intensity and larger area required for NIF experiments could easily set the backlighter power requirement greater than the total NIF power available.

One could consider increasing the x-ray conversion efficiency of area backlighters by switching to underdense volume emitters such as foams and gas-filled targets[47-49]. However, even for a predicted 30x increase in conversion efficiency at NIF scale (from say 0.3% to 10%) by switching from foil to volume emitters, the required fraction of laser power apportioned to such an area backlighter could still reach 40% by the above scaling arguments.

b) Point-Projection Backlighting Using Point Targets

In point-projection backlighting, a point source of x rays casts a shadow of the sample of interest at the detector[38] (see Figure 1b). The principal advantage over area backlighting is that for a given x-ray photon energy and hence given laser intensity I_L, the power requirements are greatly reduced[23], by the ratio of the point source area to the sample area (often factors of >100_). The other main advantage is that the detrimental long-range spatial structure from area backlighter nonuniformities are absent for an isotropically emitting point source. Current

techniques create a point source by firing a best-focus beam on thin wires or dot targets. However, point-projection backlighting has been less widely used up to now because area backlighter power requirements were still reasonable at Nova scale, and because of the following disadvantages:

1. The spatial resolution is determined by the hot emitting plasma size, which expands in time, degrading resolution. To counteract this effect, experiments have either used a short (<200-ps) backlighter pulse and a static detector, or timed a gated detector to view the earliest unexpanded phase of the backlighter plasma. A related disadvantage is that x-ray conversion efficiency is lowest early in time[50].
2. The small plasma-source size leads to more cooling by 2D and 3D expansion, reducing efficiency (i.e., edge effects are proportionately more important).
3. Because there are no imaging elements between the sample and detector as in area backlighting, the background contribution from sample self-emission is increased by the ratio of the sample to resolution element area. This forces point-projection experiments to view either cold samples, images at very high hν, or images in gated mode after the drive beams are off. Fortunately, many high-energy-density experiments are diagnosed under these conditions. For opacity experiments, the backlighter must be spectrally brighter than the sample of interest over a large range of wavelengths.
4. Until a true single-line-of-sight x-ray framing camera is in routine use[51-53], multiple lines of sight are required for each radiograph, translating to a separate point backlighter per frame.

The combination of the area backlighter advantages and the multitude of point-projection backlighter disadvantages has discouraged the routine use of point-projection imaging at facilities such as Nova. However, because area backlighting does not scale well to NIF, we have revisited point-projection backlighting in the following section with the aim of mitigating or eliminating several disadvantages.

c) Point-Projection Backlighting Using Pinholes

A new point-projection x-ray radiography technique has been developed that combines all the advantages in efficiency and flexibility of the previous methods. The technique uses pinholes to define the backlighter source size (see Figure 1c), thus allowing for arbitrary, long-duration backlighting with minimal laser-power requirements. The energy losses from 2D and 3D expansion are mitigated because the optimum plasma size is now set by the minimum laser spot size rather than the fiber size (for NIF, a 300-μm spot vs. a typical 10-μm-diam fiber).

In Figure 2a, we show gated, 4.7-keV x-ray point projection radiographs of a 50-μm vertical wire created by a backlit 25-μm pinhole. Line-outs (Figure 2b) across the wire show that the expected 1D resolution of 21 μm is maintained for several nanoseconds (Figure 2c). The backlighter laser power was only 0.2 TW, representing 20x less power than used by typical Nova area backlighters. The required backlighter laser power could have been further reduced, only limited by either the minimum achievable spot size or, as in this case, the conservative tolerance given to beam alignment (± 200 μm). The technique has also been used recently to image imploding foamballs and shells used for quantifying symmetry in NIF-scale hohlraums. A comparison of such data from backlit-pinhole backlighting vs. traditional area backlighting is shown in Figure 3. Clearly, the image SNR and uniformity is superior in the case of the backlit pinhole. In addition, it is interesting to note that while the backlit image of the 3-mm shell in Figure 3 used only two 3.5-ns-duration Omega backlighting beams totaling 0.15 TW in power, an area backlighting image would have required 15 TW, 3ω greater than all the laser power available from the Omega laser at that pulse length.

The new issue brought to the fore by backlit pinholes is the possibility of pinhole closure due to pinhole substrate ablation by the backlighter x rays produced at a distance p. From Figure 1c, ensuring an adequate backlighter field of view r at the sample a distance q from the pinhole requires that $p < q(s/r)$, where s is the backlighter source size. Because q is limited by beam travel and s should be minimized to reduce laser power requirements, this sets a maximum value for p and hence a minimum value for the x-ray fluence at the pinhole, which, assuming an intensity-independent x-ray conversion efficiency, is $\approx I_L \tau s^2/p^2$. The current experience at

Nova and Omega is that 25- and 50-μm pinholes do not close appreciably during 4 ns of 4.7-keV irradiation from plasmas created by a 0.15-TW, 400-μm-diam laser spot at p = 500 μm. Scaling to NIF, with $s_{\min}$ = 250 μm, $q_{\max}$ = 5 cm, and assuming a required field-of-view $r \approx 5$ mm sets p_{NIF} = 2.5 mm. Hence, for the same duration backlighter pulse length and same x-ray fluence at the pinhole, the backlighter power at NIF could be increased by ~25x (i.e., to 4-TW) levels without increased risk of closure. For smaller pinholes, the effects of closure can be mitigated by limiting the duration of the backlighter x rays, by tamping the pinholes with low-Z materials, or by allowing for some closure during the experiment.

We note that the 64x increase in backlighter intensity is entirely consistent with the $4^{1.5}$x larger stand-off distances that will be required for NIF diagnostics. The 25x power increase is also consistent with the idea that only a single 3-TW NIF beam per frame will be required when using backlit pinholes, at least for the mid-keV backlighting range.

III. Pinhole and Slit Arrays

For NIF, the assumption so far has been that the number of photons per resolution element can be maintained fixed at a more distant detector by increasing the backlighter laser intensity and hence x-ray intensity. However, increasing laser intensity can lead to over-driven plasmas, which suffer from reduced absorption due to parametric laser–plasma instabilities, reduced x-ray conversion efficiency at the photon energy of interest, and production of unwanted, higher-energy penetrating photons. One alternative to increasing laser intensity is to collect more photons by creating redundant images. If the sample to be backlit is nonrepeating (such as an implosion), one can use a pinhole array to produce several nonoverlapping images that later can be summed[36] electronically to improve SNR. If the sample to be backlit has a repeating pattern (such as a single-mode Rayleigh–Taylor-type experiment), then one can constructively add images directly onto the detector by an appropriate choice of pinhole or slit array separation. For example, Figure 4 shows that if the pinhole or slit separation is set at

$M/(M\pm1)$ of the wavelength of the feature of interest, where the + (–) is for area (point-projection) backlighting, respectively, then the signal can be increased by a factor of n, where n is the number of slits or pinholes.

The use of even short slits (<300 μm long) rather than pinholes for imaging 2D sample features (such as planar interfaces[4] and ridge modulations[2]) is recommended when photons are scarce, because a factor of 10x increase in collection efficiency is easily realized with minimal rotational-tolerance requirements on the slit. We note that the slits can be used either in the traditional manner with area backlighters or to provide line-projection backlighting.

IV. Backlighter Sources

Besides increasing the collected photon flux, one can work at increasing the emitted backlighter photon flux. A second alternative to increasing incident laser intensity as a means of increasing backlighter photon flux is to create distributed or spectrally broader sources.

a) Distributed, Polychromatic Backlighters

Many beam facilities such as Omega and NIF are ideally suited for creating distributed backlighter sources. Figure 5a shows an example of a configuration using stacked foils. This scheme has the advantage of providing more photons without the above-mentioned problems associated with driving just one foil. In particular, the use of multiple foils allows flexibility in setting the optimum laser intensity for producing a given photon energy source. Clearly, the flux at the detector will be optimized if there is no reabsorption as the radiation passes through intervening foils, a particular concern for commonly used resonance line radiation. Because the vast majority of backlighter experiments do not require monochromatic sources (just spectrally well understood sources), one possibility is to make each foil of a slightly different element,

stacked in such a way that each intervening foil is transparent to the characteristic radiation of the previous foils.

The example shown in Figure 5a is for K-shell emitters, where foil thicknesses need only be as thin as 10 μm. The backlighter concept of irradiating a thin foil from both sides has already been demonstrated[54]. The multiple foil scheme should also work for more opaque L- (see Figures 5b and c) or M-shell emitters[27], by switching to micron-thick coatings on low-*Z* substrates. Besides providing higher x-ray fluxes when necessary, these backlighter schemes should be useful for point-projection spectroscopy studies of interface hydrodynamics and for opacity studies. For the latter, the polychromatic M-shell backlighter may be the solution for creating spectrally brighter backlighters, which need not be spectrally continuous, over a range of photon energies below ~4 keV.

b) Picket-Fence Backlighters

Long-pulse (>500-ps) laser backlighters have been found to be more efficient than shorter-pulse backlighters for photon energies <10 keV[21,50]. This is generally attributed to better laser coupling[55-57] in the longer-scale-length plasmas that are allowed to develop with a longer pulse. Coupling this fact with the desire to operate at peak laser power without approaching peak-laser-fluence damage concerns suggests a picket-fence backlighter approach. Figure 6a shows an example of a streaked x-ray spectrum from a Nova 1-TW, 2ω picket-fence laser beam irradiating a Zn disk at 3×10^{15} W/cm^2. The first 500-ps picket produces a monochromatic He-like emission line at 9 keV. The second and third pulses at 4-ns intervals interact with a pre-expanded volume of Zn ions to produce a broadband x-ray source, with up to 3x more brightness and efficiency when integrated over the 8.5- to 9.5-keV spectral range (see Fig. 6b).

IV. Detectors

Until recently, x-ray film was used for short-pulse backlighting. Framing cameras based on microchannel plates (MCPs)[58-60] equipped with film recording media were used for long-pulse backlighting or to reduce background levels during short-pulse backlighting[40]. In Table 1, the SNR contribution from these detectors and their subelements (where measured) is tabulated for a pixel size at the detector plane of 100 μm. This SNR has been verified to be almost independent of the signal level or detector gain; it is not associated with shot noise, which should not be a concern for a well designed experiment. The representative 100-μm pixel size has been chosen to be large compared to the spatial resolution of the detectors but small compared to the dimensions of the detector. The SNR increases roughly linearly with pixel size between the size range of detector resolution and detector dimensions. The table shows that x-ray film provides a factor of ~2 better SNR, at a level very similar to the optical film. However, it is clear from these small values of SNR that the useful spatial resolution for 2D images recorded on both static and gated detectors has been limited by noise[61] rather than by the better intrinsic resolution (30-40 μm for MCPs [62-64] <5 μm for film).

a) Removal of Film Random Noise

To reduce random noise levels, the x-ray film used for static backlighting has been gradually replaced by x-ray charge-coupled-device (CCD) detectors. Similarly, the optical film used as recording medium for MCP-based framing cameras has been replaced by optical CCDs[65]. While the SNR for film is characteristically a constant[61], the absolute value of the CCD noise is characteristically a constant, as determined by the dark noise level. For a typical 9-μm-pixel optical CCD in use at Omega, the random dark noise is 20 counts compared to an optimized exposure level (i.e., approaching MCP saturation) of 20,000 counts. Averaged over a 100-μm spatial scale, the CCD SNR is hence ~10,000, a >500x improvement over the film SNR (see Table 1). Even at a few percent of maximum exposure level, the CCD SNR is still an order of magnitude greater than for film. Adding prompt data viewing and analysis capabilities and at

least as good a dynamic range to the SNR advantage, we see CCDs as clearly desirable for replacing film in all future backlighting experiments.

b) Removal of MCP Fixed-Pattern Noise

In Table 1, we note that the SNR for MCP-based film data is smaller than the film SNR on its own. We have recently discovered that this additional noise source in photon-rich MCP-based framing camera data is repeatable on spatial scales as small as 20 μm (see Figure 7a). This noise can be removed on any data by dividing, pixel by pixel, by a uniformly illuminated test image (i.e., by flatfielding[66]). An example of the improvement in uniformity before and after flatfielding is shown in Figure 8. The noise is associated with nonuniformities in phosphors prodced at LLNL. The improvement in SNR accomplished so far through such flatfielding is also given in Table 1 for both film and CCD as the recording medium.

In summary, the combination of flatfielding MCP-based data and switching to CCD as recording medium can increase SNR by close to an order of magnitude. We anticipate that this will improve gated backlighting data quality for a wide variety of experiments at Omega and NIF. Moreover, the recent retro-trend of using static x-ray CCDs to avoid gated-detector fixed-pattern noise can now be reversed. Clearly static detection has limitations; it is not applicable in those experiments where the time-integrated noise from sample self-emission and target background emission exceeds the backlit image exposure level. The discovery of how to provide high-SNR gated imaging also paves the way for long-pulse, point-projection, backlit-pinhole backlighting to perhaps become the backlighting method of choice for NIF.

V. Summary

X-ray backlighting is a powerful tool for diagnosing a large variety of high-energy-density phenomena. Traditional area backlighting techniques used at Nova and Omega cannot be extended efficiently to NIF-scale. New, more efficient backlighting sources and techniques are

required and have begun to show promising results. These include a backlit-pinhole point-projection technique, pinhole and slit arrays, distributed polychromatic sources, and picket-fence backlighters. In parallel, there have been developments in improving the data SNR and hence quality by switching from film to CCD-based recording media and by removing the fixed-pattern noise of MCP-based cameras.

Some of these new backlighting concepts have already been validated at the Omega facility. We have demonstrated the backlit pinhole concept[67] for pinholes as small as 5 μm, and quantified the improvements in flux available from distributed polychromatic sources[68].

VI. Acknowledgments

The authors thank the Operations crews of the Nova and Omega facilities, and support from the Z-Beamlet project for the picket-fence backlighter development.

References

1. J.D. Kilkenny, *Phys. Fluids B* **2**, 1400 (1990).
2. B.A. Remington et. al., *Phys. Rev. Lett*. **67**, 3259 (1991).
3. S.G. Glendinning et. al., *Rev. Sci. Instrum*. **70,** 536 (1999).
4. B. A. Hammel et. al., *Phys. Fluids B* **5**, 2259 (1993).
5. D.H. Kalantar et. al., *Rev. Sci. Instrum*. **68**, 814 (1997).
6. W.W. Hsing and N.M. Hoffman, *Phys. Rev. Lett*. **78**, 3876 (1997).
7. S.G. Glendinning et. al., *Phys. Rev. Lett*. **80**, 1904 (1998).
8. B. Yaakobi, D. Shvarts, R. Epstein, and Q. Su, *Lasers and Part. Beams* **14**, 81 (1996)
9. V.A. Smalyuk et. al., *Phys. Rev. Lett*. **81**, 5342 (1998).
10. S.J. Davidson et. al., *Appl. Phys. Lett*. **52**, 847 (1988).
11. J. Balmer et. al., *Phys. Rev. A* **40**, 330 (1989).
12. C. Chenais-Popovics et. al., *Phys. Rev. A* **40**, 3194 (1989).

13. J. Bruneau et. al., *Phys. Rev. Lett*. **65**, 1435 (1990).

14. J.M. Foster et. al., *Phys. Rev. Lett*. **67**, 3255 (1991).

15. D.M. O'Neill et. al., *Phys. Rev. A* **44**, 2641 (1991).

16. T.S. Perry et. al., *J. Quant. Spectrosc. Radiat. Transfer* **54**, 317 (1995).

17. C.A. Back et. al., *J. Quant. Spectrosc. and Rad. Trans.* **58**, 415 (1997).

18. L.B. Da Silva et. al., *Phys. Rev. Lett*. **69**, 438 (1992).

19. P.T. Springer et. al., *Phys. Rev. Lett*. **69**, 3735 (1992).

20. D.L. Matthews et. al., *J. Appl. Phys*. **54**, 4260 (1983).

21. D.W. Phillion and C.J. Hailey, *Phys. Rev. A* **34**, 4886 (1986).

22. O. L. Landen, E. M. Campbell, and M. D. Perry, *Opt. Commun.*. **63**, 253 (1987).

23. B.H. Failor, E.F. Gabl, R.R. Johnson, and C. Shepard,*J. Appl. Phys*.. **66**, 1571 (1989).

24. A.A. Hauer, N.D. Delamater, and Z.M. Koenig, *Lasers and Part. Beams* **9**, 3 (1991).

25. K. Eidmann and W. Schwanda, *Lasers and Part. Beams* **9**, 551 (1991).

26. R.L. Kauffman, *Physics of Laser Plasma*, Eds. A. Rubenchik and S. Witkowski, (North-Holland, Amsterdam, 1991) pp. 111-162.

27. P. Mandelbaum et. al., *Phys. Rev. A* **44**, 5752 (1991).

28. J.D. Molitoris et. al., *Rev. Sci. Instrum*. **63,** 5104 (1992).

29. S.G. Glendinning et. al., *Ultrahigh- and High-Speed Photography, Videography, and Photonics*, , Ed. G. Kyrala (SPIE, Bellingham, 1995) Vol. 2549, p. 38.

30. D. Attwood, B.W. Weinstein, and R.F. Wuerker, *Appl. Opt.* **16**, 1253 (1977).

31. P.M. Bell et. al., *Ultrahigh- and High-Speed Photography, Videography, and Photonics*, , (SPIE, Bellingham, 1989) Vol. 1155, p. 430

32. J.-P. LeBreton et. al., *Ann. Phys.- Paris* **19**, 87 (1994).

33. H. Azechi et. al., *Appl. Phys. Lett*. **37**, 998 (1980).

34. O.L. Landen, *Rev. Sci. Instrum*. 63, 5075 (1992).

35. J.A. Koch et.al., *Appl. Opt*. **37**, 1784 (1998) 1784.

36. J.A. Koch et. al., *Rev. Sci. Instrum*. **70**, 525 (1999).

37. B. A. Remington, B. A.Hammel, O. L. Landen, and R. A. Pasha, *Rev. Sci. Instrum*. **63**, 5083 (1992).
38. C.L.S. Lewis and J. McGlinchey, *Opt. Commun*. **53**, 179 (1985)
39. T.S. Perry et. al., *Phys. Rev. Lett*. **67**, 3784 (1991).
40. K.S. Budil et. al., *Rev. Sci. Instrum*. **68,** 796 (1997).
41. B. Yaakobi and A.J. Burek, *IEEE J. Quantum Elect*. **19**, 1841 (1983).
42. E. Forster, K. Gabel, and I. Uschmann, *Lasers and Part. Beams* **9**, 135 (1991).
43. F.J. Marshall and Q. Su, *Rev. Sci. Instrum*. **66**, 725 (1995).
44. R. Kodama et. al., *Opt. Lett*. **17**, 1321 (1996).
45. N.M. Ceglio, *Lasers and Part. Beams* **9**, 71 (1991).
46. O.L. Landen, Ed., "NIF Diagnostic Damage and Design Issues", Lawrence Livermore National Laboratory, CA, UCRL-ID-134644 (1999).
47. R.L. Kauffman, L.J. Suter, H.N. Kornblum, and D.S. Montgomery, *ICF Quarterly Report*t **6(**2), 43-48, Lawrence Livermore National Laboratory, CA, UCRL-LR-105821-96-2 (1996).
48. L.J. Suter, R.L. Kauffman, J.F. Davis, and M.S. Maxon, *ICF Quarterly Report* **6**(3), 96-102, Lawrence Livermore National Laboratory, CA, UCRL-LR-105821-96-3 (1996).
49. L.J. Suter, O.L. Landen, and J. Koch, *Rev. Sci. Instrum*. **70**, 663 (1999).
50. R. Kodama, T. Mochizuki, K.A. Tanaka, and C. Yamanaka, *Appl. Phys. Lett*. **50**, 720 (1987).
51. R. Kalibjian and S.W. Thomas, *Rev. Sci. Instrum*., **54**, 1626 (1983).
52. N. Finn, T.A. Hall, and E. McGoldrick, *Appl. Phys. Lett*. **46**, 731 (1985).
53. W. Sibbett et. al., *Rev. Sci. Instrum*. **61**, 717 (1990).
54. R.E. Turner et. al., Phys. of Plasmas **7**, 333 (2000).
55. M.H. Key, *Phil. Trans. R. Soc. London A* **300**, 599 (1981).
56. W.C. Mead et. al., *Phys. Fluids* **26**, 2316 (1983).
57. W.L. Kruer, *The Physics of Laser Plasma Interactions* (Addison-Wesley, Redwood City, 1988).
58. J.D. Kilkenny, *Lasers and Part. Beams* **9**, 49 (1991).
59. D. K. Bradley et. al., *Rev. Sci. Instrum.* **63,** 4813 (1992).

60. M. Katayama et. al., *Rev. Sci. Instrum.* **62**, 124 (1992).

61. V.A. Smalyuk et. al., *Rev. Sci. Instrum.* **70**, 647 (1999).

62. J.D. Wiedwald et. al., *Ultrahigh- and High-Speed Photography, Videography, and Photonics*, , (SPIE, Bellingham, 1990) Vol. 1346, p. 200

63. O.L. Landen et. al., *Ultrahigh- and High-Speed Photography, Videography, and Photonics*, , (SPIE, Bellingham, 1995) Vol. 2549, p. 38

64. H.F. Robey, K.S. Budil, and B.A. Remington *Rev. Sci. Instrum.* **68**, 792 (1997).

65. L.M. Logory et. al., *Rev. Sci. Instrum.* **69**, 4054 (1998).

66. D.S. Montgomery, R.P. Drake, B.A. Jones, and J.D. Wiedwald, *High-Speed Photography, Videography, and Photonics*, , (SPIE, Bellingham, 1987) Vol. 832, p. 138.

67. A.B. Bullock *et. al.*, this proceedings.

68. A.B. Bullock *et. al.*, this proceedings.

Captions

Figure 1. Schematic of backlighting configurations. a) Area backlighting, b) Point projection backlighting using point targets, and c) Point projection backlighting using pinholes.

Figure 2. a) Gated backlit pinhole radiographs at 4.7 keV of 50-μm diameter tungsten wire. Pinhole diameter is 25 μm. b) Line-out across wire radiograph at t = 1 ns (solid line), overplotted with fit (dashed line) convolving 50 μm diameter wire shadow with 21 μm FWHM source size. c) Resolution versus time for 25 μm diameter backlit pinhole (closed circles) and 40 μm diameter pinhole (open circles). Horizontal lines are predicted resolution assuming no pinhole closure.

Figure 3. Gated backlit pinhole radiograph of 3 mm-diameter Ge-doped plastic shell. Pinhole diameter is 50 μm. Inset for comparison purposes is gated radiograph from 500 μm-diameter Ge-doped plastic shell obtained using area backlighter and 15 μm pinholes.

Figure 4. Example of use of pinhole array to increase throughput when backlighting samples with repeating features. A similar scheme exists in point projection mode.

Figure 5. a) Schematic of polychromatic backlighting configuration for K-shell emitters. Each foil is transparent to its own He-like resonance line radiation and to line radiation of foils behind it. b) Schematic for L-shell emitters. c) Example of characteristic resonance L-shell line radiation from two neighboring elements (_ = 42 and 45) in the periodic table.

Figure 6. a) Streaked spectrum from picket fence backlighter. Backlighter was created by three ≈ 1 TW, 500 ps, 2_ pulses separated by 4 ns and focussed to 3×10^{15} W/cm^2 on single spot on

Zn foil. Spectrum is centered around 9 keV He-like resonance line of Zn. The weaker interleaved streaked spectrum occurring ≈ 1 ns earlier is from second lower intensity beam. b) Running spectral integral of x-ray output for each picket in arbitrary units.

Figure 7. a) and b) are two successive film images of 2 mm x 2 mm section of uniformly x-ray illuminated microchannel plate (MCP) run in dc mode. The MCP is operated at low gain (< 100) to minimize the contribution of shot noise. The two images show repeatable structure down to a 20 μm scale.

Figure 8. a) CCD image of uniformly illuminated section of MCP run at low gain in pulsed mode. b) CCD image a) divided by second uniformly illuminated image. c) Line-out across image a). d) Line-out across flatfielded image b), demonstrating 5x improvement in SNR.

Table 1. SNR at 100-μm scale for various detectors and subelements, with and without flatfielding, in the absence of shot noise. For CCD, signal approaching MCP saturation level of 20,000 counts is assumed.

Detector Element	**Raw SNR**	**SNR after Flatfield**
X-ray Film (DEF)*	18	
Optical Film (T3200)	17	
MCP + T3200	8	12
CCD	10,000	
MCP + CCD	9	>50

*DEF = Direct Exposure Film

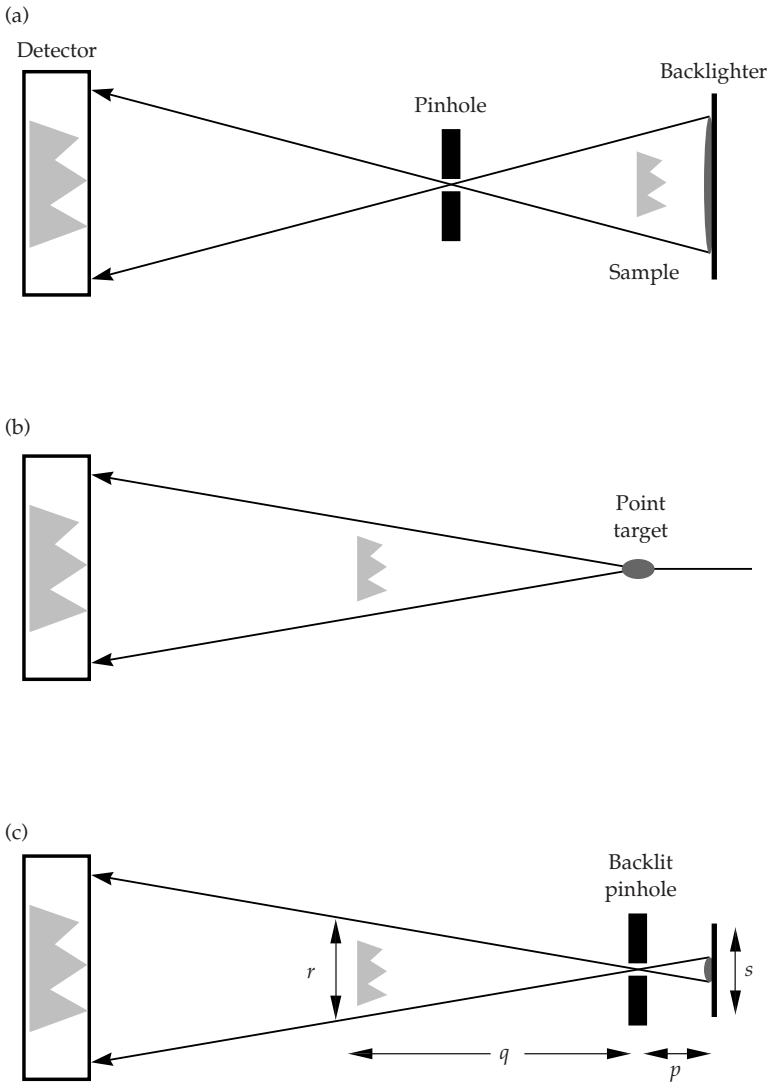
(a)
Detector
Pinhole
Backlighter
Sample
(b)
Point
target
(c)
Backlit
pinhole
r
s
q
p

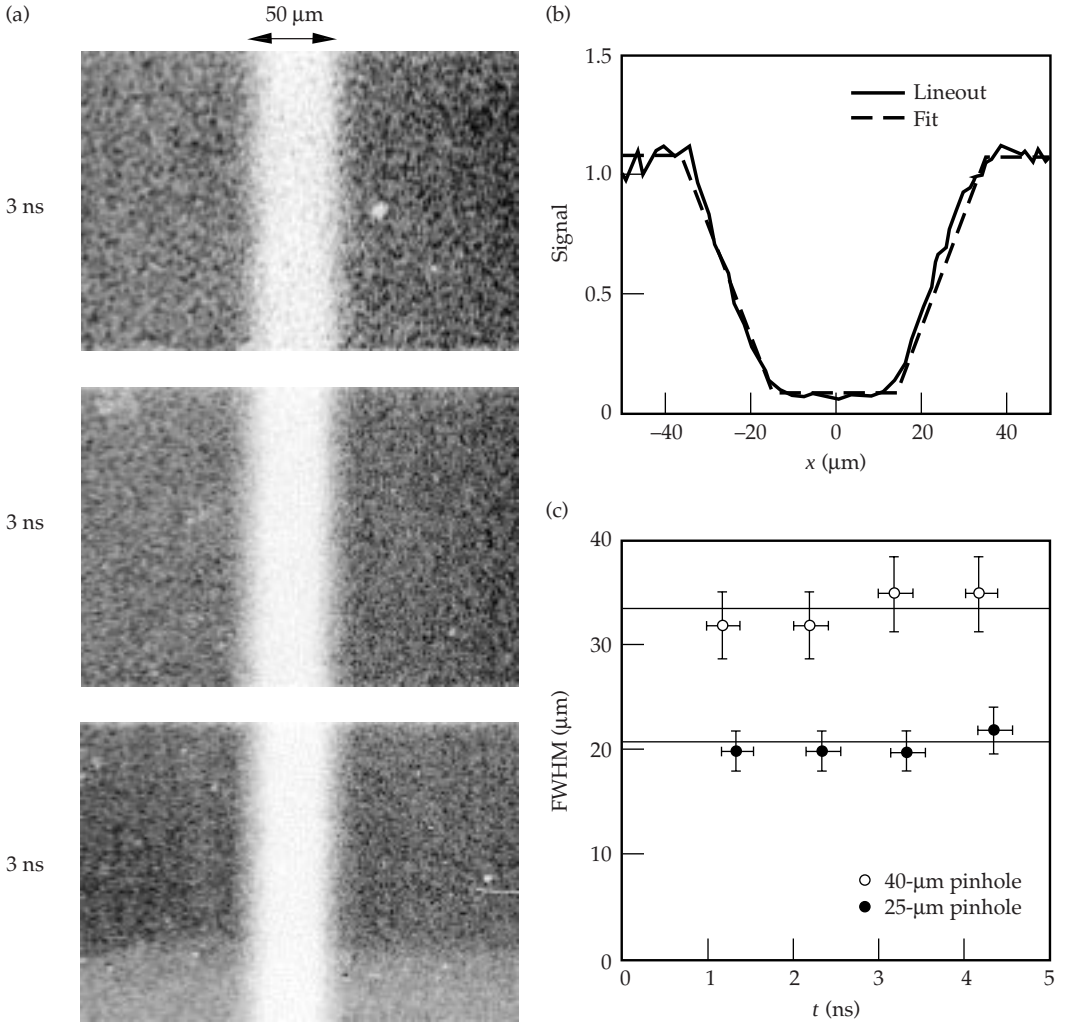
(a)
50 µm
3 ns
3 ns
3 ns
(b)
Lineout
Fit
Signal
1.5
1.0
0.5
0
–40
–20
0
20
40
x (µm)
(c)
FWHM (µm)
40
30
20
10
0
0
1
2
3
4
5
t (ns)
40-µm pinhole
25-µm pinhole

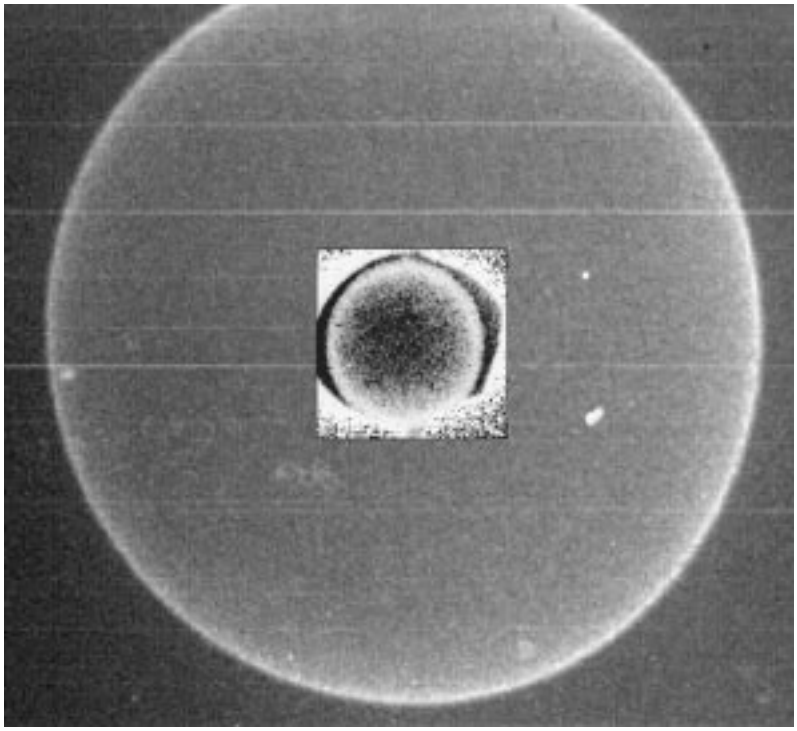

08-00-0899-1592pb01

ICF Quarterly 99/2
Lander/03
skl/8/25/99

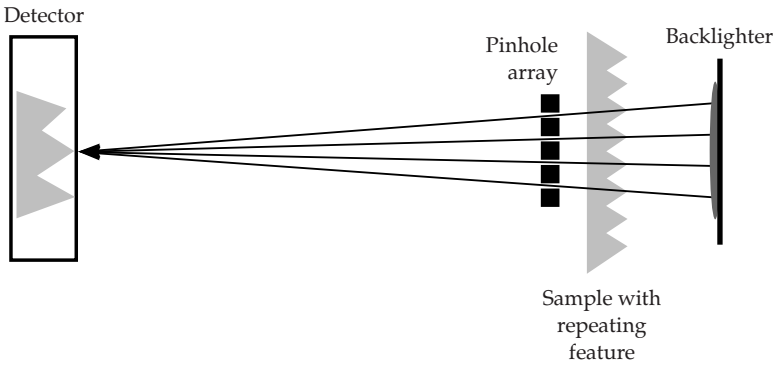

08-00-0899-1593pb01

ICF Quarterly 99/2
Lander/04
skl/8/25/99

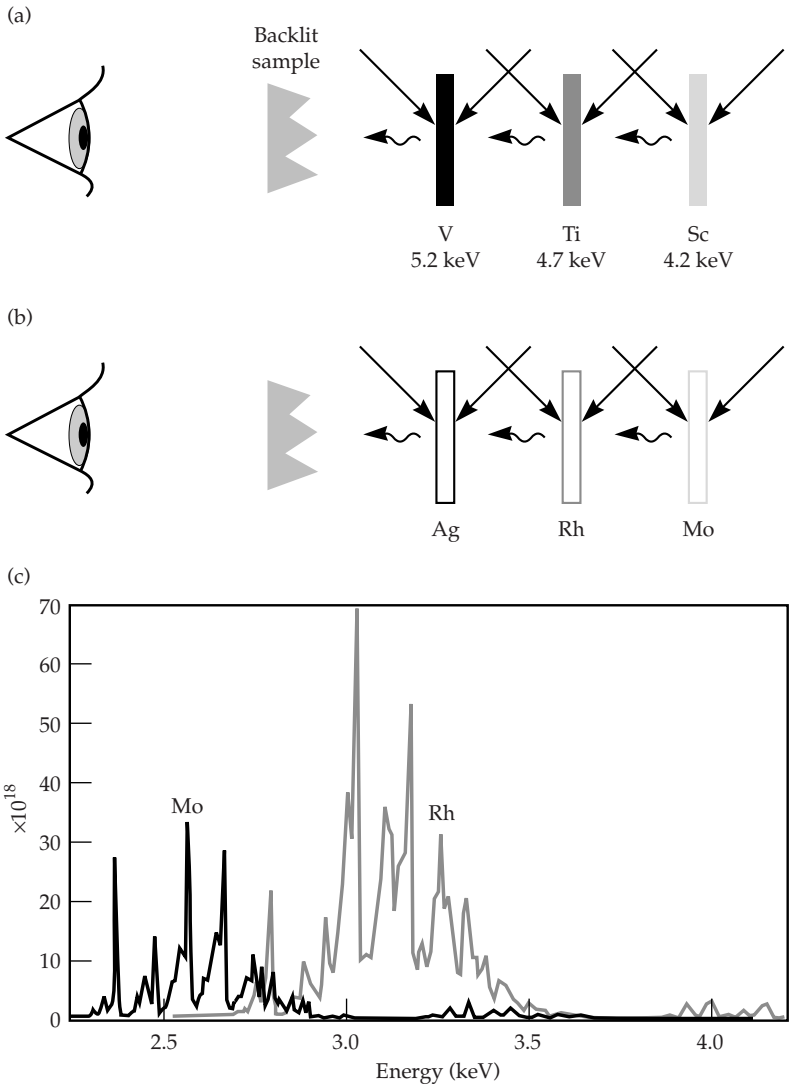

08-00-0899-1594pb01

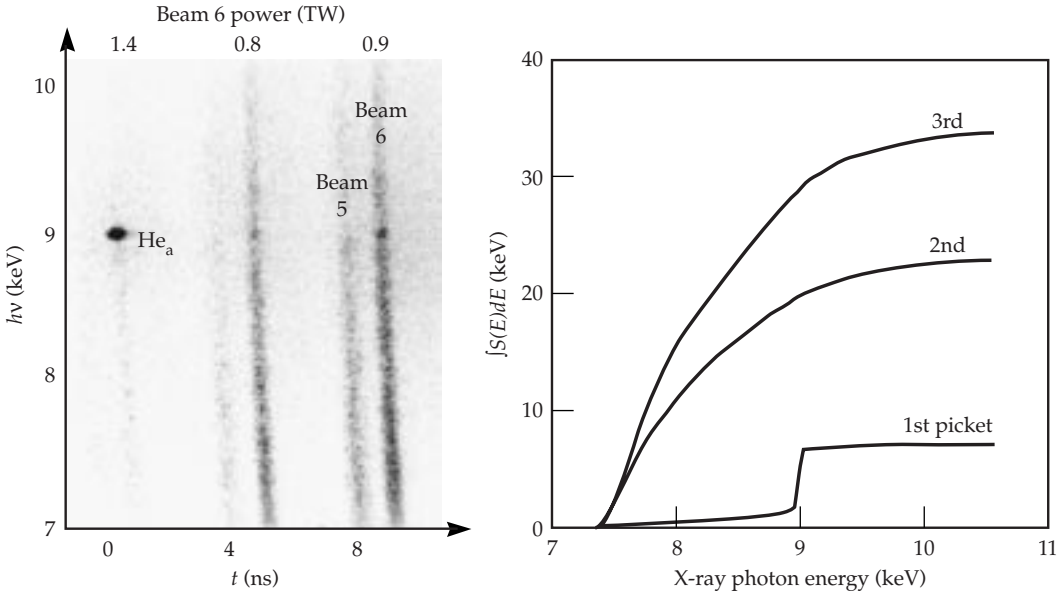

08-00-0899-1595pb01

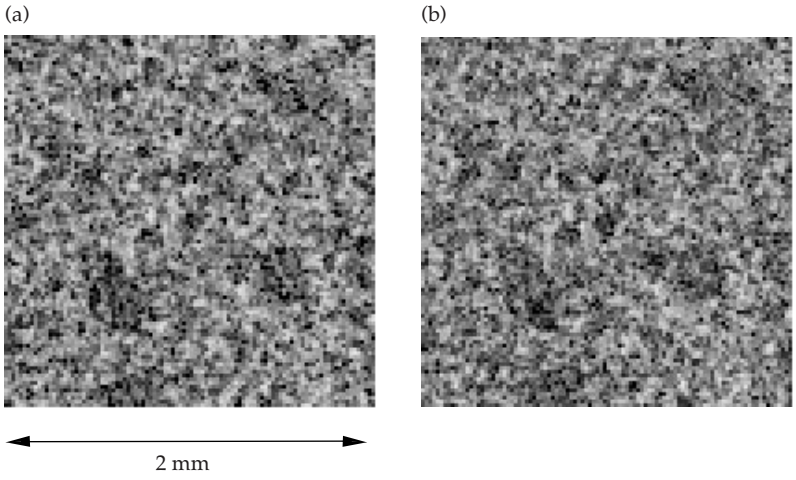

08-00-0899-1596pb01

ICF Quarterly 99/2
Lander/07
skl/8/25/99

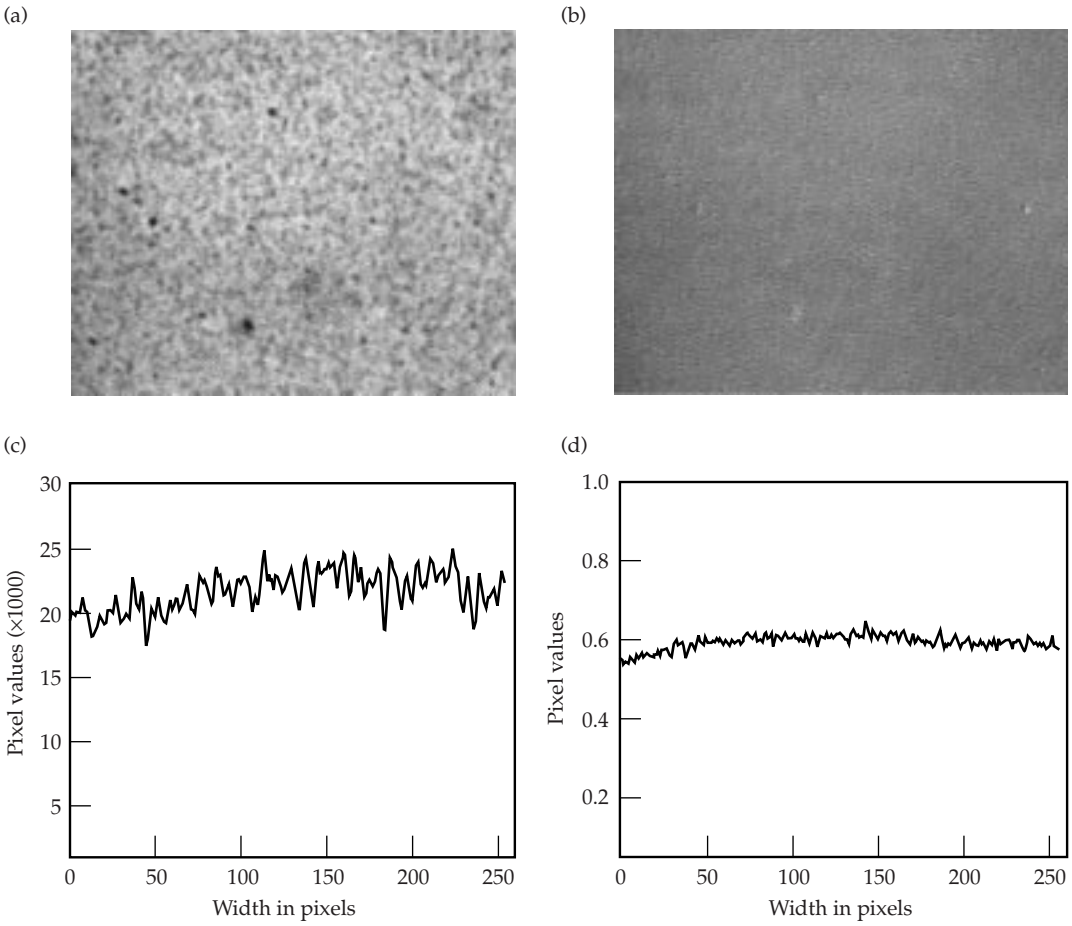
(a)
(b)
(c)
(d)
Pixel values (×1000)
30
25
20
15
10
5
0
50
100
150
200
250
Width in pixels
Pixel values
1.0
0.8
0.6
0.4
0.2
0
50
100
150
200
250
Width in pixels